Simultaneous observation of families and accompanied air showers at Mt. Chacaltaya

N. Kawasumi, I. Tsushima, K. Honda, and K. Hashimoto
Faculty of Education, Yamanashi University, Kofu, Yamanashi, 400 Japan

T. Matano
Department of Applied Physics and Chemistry, Fukui University of Technology, Fukui, 910 Japan

N. Inoue and K. Mori
Faculty of Science, Saitama University, Urawa, Saitama, 338 Japan

A. Ohsawa
Institute for Cosmic Ray Research, University of Tokyo, Tanashi, Tokyo, 188 Japan

M. Tamada
Faculty of Science and Technology, Kinki University, Higashi-Osaka, Osaka, 577 Japan

N. Ohmori
Faculty of Science, Kochi University, Kochi, 780 Japan

N. Martinic, R. Ticona, N. Gironda, F. Osco, and C. Aguirre
Instituto de Investigaciones Fisicas, Universidad Mayor de San Andres, La Paz, Bolivia
(Received 31 July 1995)

Simultaneous observations of families and accompanied air showers with emulsion chambers and the air shower array of electronic equipment at Mt. Chacaltaya (5200 m, 540 g/cm^2) reveal that families bear the data of nuclear interactions generated deep in the atmosphere. 47 outstanding families with $\Sigma E_\gamma \geqslant 10$ TeV are correlated with the accompanied air showers of the size 10^5–10^8. A scatter plot of the average family energy versus the size of the relative air shower requires further energy fractionizing process(es) in the propagation of high energy cosmic rays in the atmosphere, such as a larger dissipative mechanism in nuclear interaction, heavier chemical composition of the primary cosmic rays, etc. We reach the conclusion that nuclear interaction changes its features in the energy region $E_0 > 10^{16}$ eV, because the heavier composition, proposed so far, is not sufficient for the required dissipative process. A comparison with the data from the HADRON experiment at a similar altitude with a similar technique shows that no larger deviations are present between both experiments.

PACS number(s): 13.85.Tp, 13.85.Hd, 96.40.De, 96.40.Pq

I. INTRODUCTION

It has been reported by several groups that the family intensity, measured by the emulsion chamber located at a high mountain, is several times lower than that expected from the intensity of the primary cosmic rays [1]. This experimental result, in agreement among the experimental groups, leads to various speculations which cause further energy dissipation to the cosmic-ray propagation in the atmosphere, such as that the primary cosmic rays change its composition, that the nuclear interaction changes its feature, etc. The final conclusion, however, has not been reached so far.

This is an important problem in view of both the high-energy particle physics and astrophysics, because the energy region concerned is several times higher than the energies of the present high-energy accelerators and coincides with the so-called ''knee'' region where the primary cosmic-ray spectrum has a bend.

Taking into account the fact that the primary cosmic-ray spectrum, employed in the above analysis, is obtained by air shower experiments, we can formulate the problem from another side. A primary cosmic-ray particle of mass number A and energy E_0, incident upon the atmosphere, produces large nuclear and electromagnetic (NEM) cascades in the atmosphere [2]. An air shower experiment observes the whole of the particles, produced in the NEM cascade, while an emulsion chamber experiment observes respective high-energy particles ($>$ several TeV) among them. That is, both experiments observe the same phenomenon (NEM cascade) at a different cut edge.

It is obvious that the conventional analysis, where both data by the air shower experiment and by the emulsion chamber experiment, carried out independently, are compared through a medium of a simulation, is far from complete. The combination of both experiments enables us to observe the air showers and families without losing their correlations, i.e., what kinds of an air shower and a family are produced in a single NEM cascade. It increases the amount of information considerably and reduces the possible ambiguities inherent to the indirect comparison.

The first experiment of this kind was carried out by Smorodin *et al.* [3] at an airplane altitude in the early 1960s in order to investigate the nucleon interactions at energies above 10^{13} eV. We started in 1968 the experiment of emul-

TABLE I. Experiments operating with the emulsion chamber and the air shower array at high mountains.

Experiment	Start	Mountain (height, depth)	Emulsion chamber (1) Area (2) Thickness	Air shower array (1) Density detectors (area) (2) Core detector (3) Burst detector	Statistics of the events (definition of the family)
AS_γ [5,7]	1968	Mt. Norikura (2700 m, 738 g/cm^2)	(1) 20 m^2 (2) 14 c.u. Fe	(1) 32 scintillators (R=40 m) (2) Spark chamber (54 m^2) (3) Scintillator (18 m^2)	99 events ($\Sigma E_{\gamma,H} \geq 10$ TeV, $n_{\gamma,H} \geq 2$, $E_{\gamma,H} \geq 2$ TeV)
SYS [4]	1979	Mt. Chacaltaya (5200 m, 540 g/cm^2)	(1) 8 m^2 (2) 30 c.u. Pb	(1) 44 Scintillators (R=50 m) (2)— (3) Scintillator (8 m^2)	47 events ($\Sigma E_\gamma \geq 10$ TeV, $n_\gamma \geq 5$, $E_\gamma \geq 2$TeV)
HADRON [6]	1985	Tien Shan (3300 m, 700 g/cm^2)	(1) 162 m^2 (2) 12 c.u. Pb+70 g/cm^2 C +10 c.u. Pb	(1) 28 scintillators (R=70 m) (2)— (3) Ionization chambers (162 m^2)	1531 events ($\Sigma E_\gamma \geq 10$ TeV, $n_\gamma \geq 2$, $E_{\gamma,H} \geq 2$ TeV)

sion chambers associated with burst detectors, installed under the 20 m^2 spark chamber, in the central area of a Tokyo air shower array in the Institute for Nuclear Study, University of Tokyo, in order to study high-energy hadrons and large transverse momentum phenomena in air showers. Then the detectors were moved to Mt. Chacaltaya in 1977 for the present experiment (SYS) [4]. Dake *et al.* started the experiment at Mt. Norikura in 1968 to study multicore events of air showers and families (ASγ) [5], and the large scale experiment HADRON started at Tien Shan in 1985 [6]. (See Table I.) The SYS experiment is a unique one of this sort under operation at present.

The ASγ experiment at Mt. Norikura drew the conclusion that a proton's fraction is poor, i.e., 20% at $E_0=1.4\times10^{15}$ eV, among the primary cosmic-ray composition (consequently the composition becomes heavier than that in a low-energy region, where the proton fraction is 40–50%), by comparing the frequency of families with $\Sigma E_{\gamma,H}$ (the total observed energy in the family) in the experiment and in the simulation [5,7]. Recently they made a reanalysis of their data to confirm the above-mentioned conclusion [10]. As shown in Table II, however, the estimation of the primary cosmic-ray composition by the intensity argument depends on the assumed model of nuclear interaction. It was pointed out [12] that the energy spectrum of produced particles, assumed in their simulation code, shows weaker violation of the Feynman scaling law [13] than that observed by the accelerator experiments.[1] Therefore, if they assume the energy spectrum, consistent with the data by accelerator experiments, in their simulation code leaving other features of nuclear interactions untouched, they would reach a conclusion of less heavy-dominant composition. Some comments will be given in Sec. IV on the ASγ experiment.

The HADRON experiment at Tien Shan, in the preliminary report, concludes that the primary cosmic-ray composition is a mixed one (a heavy composition in our vocabulary, defined in the remark in Table II) from the normalized integral size spectrum of air showers which are accompanied by families [6]. There is, however, a discrepancy of absolute value between the above-mentioned spectrum by the experiment and that by the simulation. Recent results of the HADRON experiment [15] will be discussed in Sec. III of this paper in relation to the data of our experiment, respectively, because their way of analysis is similar to ours.

The present paper consists of four sections. Section II describes the experimental setup and the experimental procedure. Section III presents the experimental results to show the origin of the families in relation to the air showers and to conclude that the change of the nuclear interaction is necessary for the required rapid energy dissipating process. Section IV is devoted to a summary and discussion on the content of the change of the nuclear interaction, on the assumptions in the simulation, and on the future prospect of the experiment.

II. THE SYS EXPERIMENT

The experiment operating an emulsion chamber and an air shower array together at Mt. Chacaltaya was started in 1979 by the SYS Collaboration (Saitama University and Yamanashi University in Japan, and Universidad Mayor de San Andres in Bolivia) [11]. The geographic parameters of the Cosmic Ray Laboratory at Mt. Chacaltaya (Bolivia) are height, 5200 m (540 g/cm^2 of atmospheric depth), location, 16°21′ S, 68°08′ W.

The initial motivation for the experiment was to obtain the information on the primary particle interaction that produces the air shower, by observing the high-energy hadrons and γ rays in the air shower via the emulsion chamber. It depends on the consideration that most of the high-energy particles, observed by the emulsion chamber, come directly from the same interaction that initiates the air shower. It will be shown in Sec. III of this paper that this assumption is too simplified.

A. Experimental setup

1. Air shower array

The configuration of detectors of the air shower array is shown in Fig. 1. The array covers an area of radius R=50 m by 35 detectors of plastic scintillator, 31 detectors of 0.25

[1]Some of the authors of the ASγ experiment assert incorrectly that the x distribution, assumed in their simulation code, is consistent with the data by the accelerator experiment [10,14].

TABLE II. Conjectures on the chemical composition of the primary cosmic rays and the assumed extent of the violation of Feynman scaling law.

Author(s)	Conclusion on the composition of the primary cosmic rays[a]	Violation of Feynman scaling law in the assumed nuclear interaction model	Experimental data
Shibata [8]	Light	Strong	Fuji
	Heavy	Weak	
Ren *et al.* [9]	Heavy	Weak[b]	Fuji/Kanbala
Shima *et al.* [5,7]	Heavy	Weak[b]	Norikura
Saito *et al.* [10]	Heavy	Weak[b]	Norikura
Kempa *et al.* [11]	Light	Strong	Fuji

[a]The composition, consistent with that in the low-energy region ($<10^{13}$ eV) which has the proton fraction 40–50 %, is called "light" composition.
[b]The simulation code is the same.

m^2, and 4 of 1 m^2, to measure the lateral distribution of electron density of the air shower. And 5 plastic scintillators (0.25 m^2 each) with the fast-timing circuit are located in pyramid shape in the center of the array to measure the arrival direction of the air shower.

The recording system of the air shower array is triggered when one of the burst detectors, described below, has the density $n_b > 10^3$.

2. Emulsion chamber

32 blocks (0.25 m^2 each) of emulsion chamber are installed in the center of the air shower array (Fig. 1). A configuration of 32 blocks is shown in Fig. 2, and the structure of one unit in Fig. 3. The chamber generally consists of 30 sheets of lead plate (0.5 cm thick each), equivalent to 30 cascade units (c.u.) or 0.81 inelastic collision mean free path (λ_{inel}) in total, and of 14 sensitive layers of x-ray films inserted under every 1 cm of lead plate. Some sensitive layers contain nuclear emulsion plates besides x-ray films for the calibration of energy. [See Sec. II B 2.] The emulsion chamber detects the electron showers produced by high-energy particles incident upon the chamber, and measures their energies, positions, and directions of incidence.

Table III shows the exposure list of emulsion chambers. In 1989 the detectors of the air shower array was increased so as to cover the emulsion chamber of the Brazil-Japan Collaboration [1,16] too. Therefore the data of accompanied air showers is available for the high-energy families observed by the emulsion chambers of the Brazil-Japan Collaboration. However, the present analysis concerns the data of SYS chambers from 1979 to 1986, which have a uniform quality.

3. Burst detectors

Burst detectors of plastic scintillator (0.25 m^2 each) are installed underneath the respective blocks of the emulsion chamber (Fig. 3). A burst detector measures the number of charged particles (called "burst density" n_b) which penetrate the emulsion chamber.

When the core of an air shower hits the burst detectors, many of them have signals of the burst density and the map of the burst densities determines the center of the burst.

B. Experimental procedure

1. Size of the air shower

The lateral distribution of electron density, measured by the density detectors of the air shower array, is fitted to the

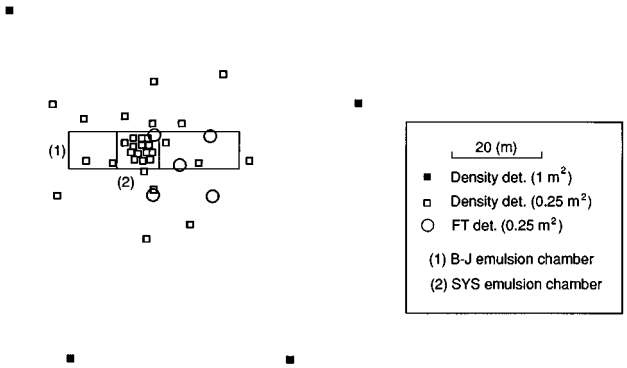

FIG. 1. Complete schema of the air shower array. 35 density detectors of plastic scintillator cover the area of the radius $R=50$ (m). The emulsion chamber is located in the room (2).

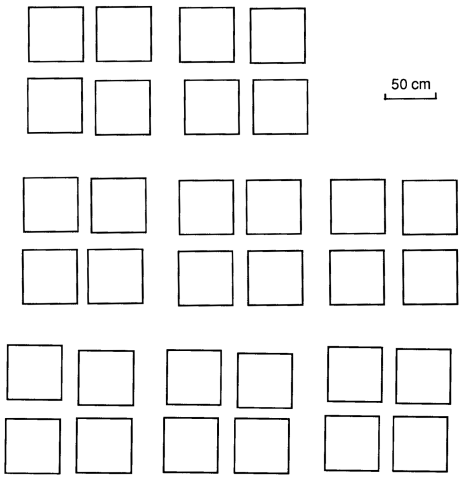

FIG. 2. Configuration of the blocks of the emulsion chamber in the room (2).

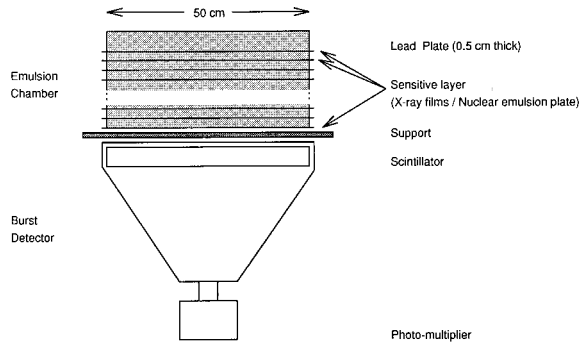

FIG. 3. Structure of the emulsion chamber and the burst detector. Each block of the emulsion chamber is 50×50 (cm^2) of area and 15 cm Pb thick with 14 sensitive layers of x-ray films, inserted at each 1 cm of lead plate. The burst detector of plastic scintillator is located underneath the emulsion chamber.

Nishimura-Kamata-Greisen (NKG) function of the Molière unit $r_0=155$ m [17] to obtain the total electron number N_e, called ''size,'' and the age parameter s of the air shower.

Figure 4 shows the size spectrum of all the observed air showers in 1982. The spectrum is consistent with the one by BASJE, another air shower experiment at Mt. Chacaltaya [18], in the size region of 5×10^5–5×10^6.

2. Energy of γ rays and hadrons [16]

A high-energy particle of electromagnetic component (electrons and photons), incident upon the chamber, produces an electron shower in the chamber through the cascade process in lead plates. Hence the photosensitive layers, inserted at various depths in the chamber, observes the various stages of shower development. The electron shower is recorded as a small black spot, visible with the naked eye, on the x-ray film after photographic development. This performance of emulsion chamber shows that the incident electron and photon cannot be discriminated, and it is the reason why they are called ''γ rays'' collectively by emulsion chamber experiment.

The routine in an emulsion chamber experiment is to measure the darkness of the spots by the microphotometer with the slit of a certain size (usually the size of 200×200 μm^2) and to make a transition curve of darkness (the development of darkness along the depth of the chamber) for each shower. Comparison of the transition curve with those of various incident energies by the cascade theory [19], determines the relative value of the energy and the starting depth Δt of the shower, because the darkness is related to the number of electrons in the shower. On the other hand, the electron number in the shower, obtained directly by the microscopic observation of the shower in the nuclear emulsion plates, determines the absolute value of the energy by comparing its transition curve with those of the cascade theory. An emulsion chamber detects the showers of the energy exceeding ~1 TeV.

In the case of hadron incidence, the shower is originated by photons (mainly through the decays of π^0's and η's) which are produced by the nuclear interaction of the hadron with the lead plate. The visible energy of the shower is not the incident energy of the hadron E_h but a fraction of it $k_\gamma E_h$

TABLE III. Exposure list of the emulsion chambers and the electronic detectors of the air shower array in SYS experiment.

Emulsion chamber			Air shower array Detectors
Series	Construction-disassembly	Area (thickness, sensitive layers, burst det./target)	
			78/04/10
I-79	79/05/29-79/11/26	8 m^2 (15 cm Pb, 14 layers, burst det.)	Density 31 (0.25 m^2)
II-0A	80/05/25-80/09/26	8 m^2 (15 cm Pb, 14 layers, burst det.)	4 (1 m^2)
III-0B	80/10/23-81/03/20	8 m^2 (15 cm Pb, 14 layers, burst det.)	FT 5 (0.25 m^2)
IV-82	82/09/16-83/08/11	8 m^2 (15 cm Pb, 14 layers, burst det.)	
V-83	83/10/07-84/08/23	8 m^2 (15 cm Pb, 14 layers, burst det.)	
VI-84	84/09/17-85/09/19	8 m^2 (15 cm Pb, 14 layers, burst det.)	
VII-85	85/11/29-86/11/25	8 m^2 (15 cm Pb, 14 layers, burst det.)	
			87/09/30
VIII-88	88/01/12-89/10/06	8 m^2 (15 cm Pb, 14 layers, burst det.)	Density 31 (0.25 m^2)
			4 (1 m^2)
			FT 8 (0.25 m^2)
IX-89-C23	89/11/11-91/03/11	8 m^2 (15 cm Pb, 14 layers[a], burst det.)	89/11/24
		46 m^2 (14 cm Pb, 5 layers[a])	Density 36 (0.25 m^2)
		38 m^2 (11 cm Pb, 4 layers[a], 60 cm C)	4 (1 m^2)
			FT 8 (0.25 m^2)
X-91-C24	91/03/16-92/10/12	8 m^2 (15 cm, Pb, 14 layers, burst det.)	91/10/25
		42 m^2 (13 cm Pb, 12 layers, 30 cm CH_2CH_2)	Density 36 (0.25 m^2)
		38 m^2 (11 cm Pb, 5 layers*, 60 cm C)	4 (1 m^2)
XI-93-C25	93/11/10-	8 m^2 (9 cm Pb, 8 layers, burst det.)	FT 8 (0.25 m^2)
		41 m^2 (9 cm Pb, 8 layers)	5 (1 m^2)

[a]Japanese and Russian X-ray films.

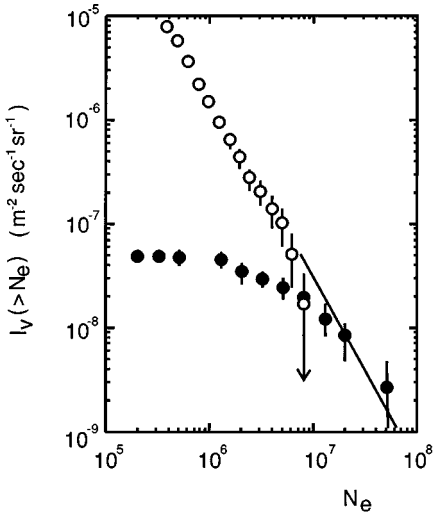

FIG. 4. Size spectrum of the air showers. Open circles are for all the observed air showers and the full circles for those which accompany the families. The solid line is the spectrum of all the air showers by BASJE, another air shower experiment at Mt. Chacaltaya.

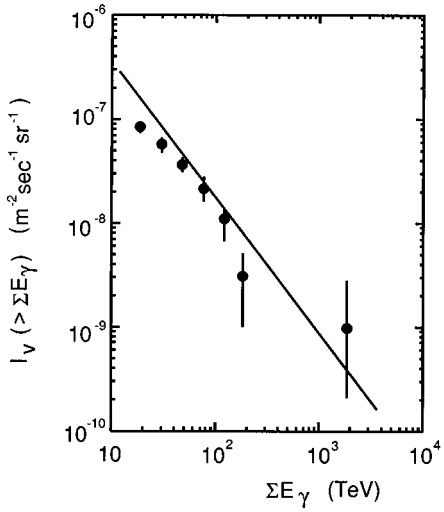

FIG. 5. ΣE_γ spectrum of the families. The solid line is the spectrum by the Brazil-Japan Collaboration, another emulsion chamber experiment at Mt. Chacaltaya. The minimum energy $E_{\min}$ is set at 4 TeV in the definition of the family for this figure, in accordance with the Brazil-Japan Collaboration.

where k_γ is the ratio of the total energy of γ rays to the incident energy of the hadron. Accordingly the detection of hadrons depends on the collision probability in the chamber, the distribution of k_γ, and the detection threshold energy of the chamber.

The showers with the starting depth $\Delta t \geqslant 6$ (c.u.) are defined as hadron-induced ones, because the probability for γ rays to have such a starting depth is $p<e^{-6}=2.5\times10^{-3}$. Those showers will be called ''hadrons'' hereafter, and the visible energy of the hadron-induced shower is expressed by $E_h^{(\gamma)}$, i.e., $E_h^{(\gamma)}=k_\gamma E_h$.

3. ΣE_γ of the family

Usually, when the emulsion chamber is hit by the core of an air shower, it detects a bundle of γ rays and hadrons in the air shower, which is called ''family.'' Identification of the showers composing the family is easy because they have the same zenith and azimuth angles on the map where trajectories of all the showers are projected on the horizontal plane.

Analyses made below are for the families which fulfill the following criteria: (1) minimum energy of the shower, $E_{\min}=2$ TeV; (2) number of γ rays, $N_\gamma \geqslant 5$; (3) total energy of γ rays, $\Sigma E_\gamma \geqslant 10$ TeV.

Figure 5 shows the ΣE_γ (the sum of γ-ray energies in the family) spectrum of the families. It agrees well with that by the Brazil-Japan Collaboration with the pure emulsion chamber at Mt. Chacaltaya [1,16], showing that energy determination of the showers is consistent in both experiments. It should be noted that the minimum energy is set 4 TeV in Fig. 5 in accordance with Brazil-Japan Collaboration.

4. Coupling the family with the accompanied air shower

Families have the data of (1) the arrival direction and of (2) the position, but not of (3) the arrival time, because the emulsion chamber is exposed to cosmic rays for 1–2 yr continuously to accumulate cosmic-ray events. On the other hand, the air showers have all three of them. It is not easy to couple the air shower with the family directly by the data of their arrival directions and their positions, because it is common that there are several candidate air showers to one family within the allowance of the experimental errors. Hence the air shower is looked for through the mediation of the data of the burst in the following way.

(1) List the families in one block of the emulsion chamber.

(2) List the bursts which have their centers on the concerned block of the emulsion chamber.

(3) Correspond the families to the bursts on the assumption that the order of magnitude of the family (ΣE_γ) is the same as that of the burst density at the center (n_b).

(4) Examine the consistency of the arrival direction between the air shower and the family, and also of the position between the air shower core and the family center.

By this algorithm 47 among 67 observed families are coupled with air showers. Hence the coupling rate is 70%, and it increases to 77% taking the dead time of the air shower array into account. For the 47 coupled events the differences of the arrival directions between the family and the accompanied air shower are 5.4 ± 0.5 (deg) for zenith angle and 17.0 ± 1.8 (deg) for azimuth angle on the average. The difference of the positions between the family center and the air shower core is 0.49 ± 0.04 (m). The coupling rate increases to 85% for the families with $\Sigma E_\gamma > 50$ TeV.

The size spectrum of the accompanied air showers is shown in Fig. 4. One sees that all the air showers accompany families in the region $N_e > 10^7$, or that the primary cosmic rays always produce the visible families in the region[2] $E_0 > 2\times10^{16}$ eV. The difference of both spectra in the high size region, observed in Fig. 4, is due to the low statistics of the events. That is, that of all the air showers is based on the data in 1982, when the triggering of the recording system is made by the air shower, and the triggering is made by the

[2]We assume 2×10^9 (eV/electron) as the factor between the primary energy and the size of the air shower. See Sec. II C 5.

TABLE IV. Chemical composition of the primary cosmic rays, assumed in the simulation.

E_0 (eV)	Proton (%)	Alpha (%)	CNO (%)	Heavy (%)	Fe (%)
10^{15}	42	17	14	14	13
10^{16}	42	13	14	15	16

burst in the experiment of simultaneous observation, starting in 1979.

C. Simulation

The principle of our simulation is to use as simple assumptions as possible without losing the essential points, because most of them are not established yet in the concerned energy region, being the themes of investigation. What follows is a brief description on our simulation procedure [20].

1. Primary cosmic rays

Energy spectrum of the primary cosmic rays is assumed to be

$$E_0^{-\gamma}$$

in the integral form. The exponent γ is ~ 1.8 at $E_0 = 10^{15}$ eV and increases gradually to 2.0 with the energy. The energy region of the primary cosmic rays to be sampled is above 10^{15} eV.

The assumed chemical composition is so-called ''normal'' one which is estimated by Nikolsky by the analysis of the experimental data of air showers [21]. (See Table IV.) It is a light composition in our vocabulary. (See the remark in Table II.)

2. Nuclear interactions

(a) Collision mean free path of hadrons in the air. The collision mean free path of hadrons in the air is assumed to be

$$\lambda_{\rm air} = 760 \sigma_{\rm inel}^{-0.63} \quad ({\rm g/cm^2}),$$

where the inelastic cross section of hadrons $\sigma_{\rm inel}$ is given by

$$\sigma_{\rm inel} = \sigma_0 [1 + 0.0273\epsilon + 0.01\epsilon^2 \theta(\epsilon)] \quad ({\rm mb})$$

with $\epsilon = \ln(E/200\ {\rm GeV})$ [22]. The constant σ_0 has different values for nucleon-nucleon ($N-N$) and pion-nucleon ($\pi - N$) collisions:

$$\sigma_0 = \begin{cases} 32.2\ {\rm mb}, & N-N, \\ 20.3\ {\rm mb}, & \pi - N. \end{cases}$$

The increasing cross section $\sigma_{\rm inel}$ reproduces the experimental data consistently in the low-energy region, giving a 10% higher estimation than the experimental value at $\sqrt{s} = 1800$ GeV [23].

(b) Hadron-air collisions. We employ UA5 simulation algorithm [24] for the model of multiple-particle production of N-air collision. It is because we assume that N-N and N-air collisions have the same features of multiple-particle production in the forward hemisphere of the collision, and because the propagation of cosmic rays in the atmosphere is governed mostly by the particles produced in the forward hemisphere. UA5 algorithm is the phenomenological simulation logic and reproduces the features of multiple particle production at $\sqrt{s} = 53$, 200, 546, and 900 GeV at the CERN super proton synchrotron (SPS) $\bar{p}p$ collider. The energy spectrum of produced particles, predicted by the algorithm, shows a fair violation of Feynman scaling law both in the forward and central regions in terms of $dN/dx = (1/\sigma_{\rm inel})\, d\sigma/dx$ with $x = p_{\parallel}/E_0$, and the inelasticity distribution is approximately uniform between 0.1 and 0.9 in the laboratory system, giving the average $\langle K \rangle = 0.40$. (See the Appendix I.)

Further additional assumptions made in our simulation code are (1) all the produced particles are pions, and (2) π-air collisions follow the same algorithm as N-air collisions. Hence one should keep it in mind that the charge-exchange process of the leading particle, $\pi^{\pm} \rightarrow \pi^0$, is not assumed.

(c) Nucleus-air collisions. The wounded-nucleon model is assumed for nucleus-air collisions [25]. That is, the number of wounded nucleons which expresses the number of nuclear interactions in the air nucleus, is given by

$$N_w = A - A' - 4N_\alpha - N_{\rm evap},$$

where A is the mass number of the incident nucleus, A' that of the fragment nucleus after the collision, N_α the number of α particles, and $N_{\rm evap}$ the number of evaporated nucleons. These quantities, A', N_α and $N_{\rm evap}$, are sampled from the appropriate distributions [20].

3. Electromagnetic interactions

For the particles of electromagnetic component (electrons and photons) with the energy exceeding 1 TeV, the processes of pair creation and bremsstrahlung without the Landau-Pomeranchuk-Migdal effect [26] are taken into account.

4. Families

Simulation for families is made in a three-dimensional way. That is, the coordinates and the energies are the available data for showers in the family. γ rays and hadrons which have visible energy exceeding 2 TeV and location within the circles of 15 cm radius from the family center, are registered as family members. The interaction probability of hadrons in the chamber is assumed to be 0.7, and the visible energy of the hadron-induced shower is given by $k_\gamma E_h$ where k_γ is sampled from the Γ distribution of $\langle k_\gamma \rangle = 0.15$.

5. Air showers

The simulation for the air showers is made in a one-dimensional way, and therefore only the size N_e is the directly available data.

Hadrons are traced down following the algorithm of nuclear interaction until their energies become 0.1 TeV or

TABLE V. Statistics of the simulated events.

No. of simulated primaries ($E_0 > 10^{15}$ eV)	23 452
No. of families by the simulation	13 274
No. of families by the criteria	8 157

they arrive at the observation level of Mt. Chacaltaya. Those with the energy less than 0.1 TeV are assumed to have no further interaction, because the majority of them are pions that decay into muons.

Electrons with an energy less than 1 TeV are replaced by the analytic solution of electron number by the cascade theory under Approximation *B* [19] instead of being traced down by the algorithm of electromagnetic interactions. However, photons are traced down until they convert to electron pairs, their energies become the critical energy in the air (80 MeV), or they arrive at the observation level.

The size of the air shower N_e is defined as the total number of charged particles which arrive at the observation level (Mt. Chacaltaya) among those produced by the above processes. The air shower size, thus defined, reproduces the well-known relation $E_0/N_e \simeq 2.0$ GeV on the average with a narrow dispersion of the distribution[3] [20].

6. Statistics

Table V shows the statistics of the simulated events.

III. EXPERIMENTAL RESULTS

A. Energy spectrum of γ rays in one family

Energy spectra of γ rays in one family, by experiment and by simulation, are shown in Fig. 6 for three different size regions of $N_e = 10^5$–10^6, 10^6–10^7, and 10^7–10^8. The experimental data show that the spectra of different N_e regions differ in the number of γ rays in one family. Comparison of the spectra in the experiment and in the simulation shows that there is a discrepancy in the number of γ rays, i.e., the experiment gives a smaller number than the simulation, while the slopes of the spectra agree with each other. Meaning of the discrepancy will be discussed in Sec. III C.

The experiment HADRON at Tien Shan reported that the spectrum, expressed by the variable $x = E_\gamma/E_0$ where E_0 is estimated from N_e by assuming $E_0/N_e = 2.0$ GeV, becomes steeper suddenly in the size region exceeding 10^7, compared with those in lower size region [15]. And they argue that nuclear interaction changes its feature at $\sim 2\times10^{16}$ eV. However such a change of the slope is not observed in Fig. 6 by our experiment.

In order to study the relation between the families and the accompanied air showers in more detail, we compare the energy spectra of γ rays in one family, grouping the events both by ΣE_γ and N_e. That is, all the families with $\Sigma E_\gamma = 10$–215 TeV are classified into four groups of $\Sigma E_\gamma = 10$–21.5, 21.5–46.4, 46.4–100 and 100–215 TeV. Figure 7 shows the energy spectrum of γ rays in one family, for two groups of events with the same interval of $\Sigma E_\gamma = 46.4$–100 TeV but with different intervals of $N_e = 10^5$–10^6 and 10^6–10^7, as an example. As can be seen in the figure, the energy spectra of the same interval of ΣE_γ agree well with each other in spite of the difference of size region. In other words, the energy spectrum of γ rays in one family does depend on ΣE_γ of the family, but does not on N_e of the accompanied air shower. It is the case in the simulation, too.

It indicates that the family is produced deep in the atmosphere by a small number (one or two) of interactions of high-energy hadrons in the air shower. Therefore there is no sharp correlation between the characteristics of the family and those of the accompanied air shower.

Figure 8 presents the energy spectra of γ rays in one family for four intervals of ΣE_γ without classifying the events by N_e to improve the statistics. On the whole the spectra in the experiment and in the simulation agree with each other with respect to both the slope and the number of γ rays.

B. Energy spectrum of hadrons in one family

The energy spectrum of hadrons in one family is shown in Fig. 7(b) for two groups of events with the same interval of $\Sigma E_\gamma = 46.4$–100 TeV but with the different intervals of $N_e = 10^5$–10^6 and 10^6–10^7. Figure 9 shows the energy spectrum of hadrons in one family for four intervals of ΣE_γ. These figures of hadrons confirm what are mentioned for the γ rays in the family, i.e., the agreement of the energy spectra in one family for the families belonging to the same interval of ΣE_γ in spite of the different intervals of N_e, and the agreement of those by the experimental data and by the simulation for the families belonging to the same intervals of ΣE_γ.

Comparison of Figs. 9(a) and (b) shows that only the spectrum of the highest ΣE_γ interval, i.e., $\Sigma E_\gamma = 100$–215 TeV, deviates from that by the simulation, though the statistics is not sufficient yet. The observed increase of hadrons in the family may have some relation with the change of nuclear interaction in high-energy region, which will be discussed elsewhere with better statistics of high-energy events.

To conclude the present and previous subsections, our simulation code does simulate the features *inside* the family well, but does not the relation between the family and the air shower (or between the family and the primary energy of the event).

C. Correlation between $\langle \Sigma E_\gamma \rangle$ and N_e

Figure 10 shows the correlation between ΣE_γ and N_e. Figure 11 shows the dependence of the average value of ΣE_γ

[3]The distribution of E_0/N_e is not symmetric around the average value, having a long tail on the larger value side than the average on the log scale as well as on the normal scale, due to the large fluctuation of the starting points of air showers. Hence we will describe the distribution in terms of the average and the standard deviation, defined by $\sigma \equiv \sqrt{\langle x^2 \rangle - \langle x \rangle^2}$.

E_0	Primary particle	Distribution of E_0/N_e Average (GeV)	σ (GeV)	Remarks
$1-1.5\times10^{15}$ eV	p	1.95	0.62 (32%)	Events with $E_0/N_e > 5$ (GeV) are omitted
$1-1.5\times10^{15}$ eV	Fe	2.08	0.09 (4.3%)	

The sampled events are all the air showers, irrespective of the accompaniment of the families. The value is consistent with "31% (standard deviation) at $N_e = 5\times10^5$ for the proton-dominant (PD) composition" in the simulation for Yangbajing (4300 m) experiment [10].

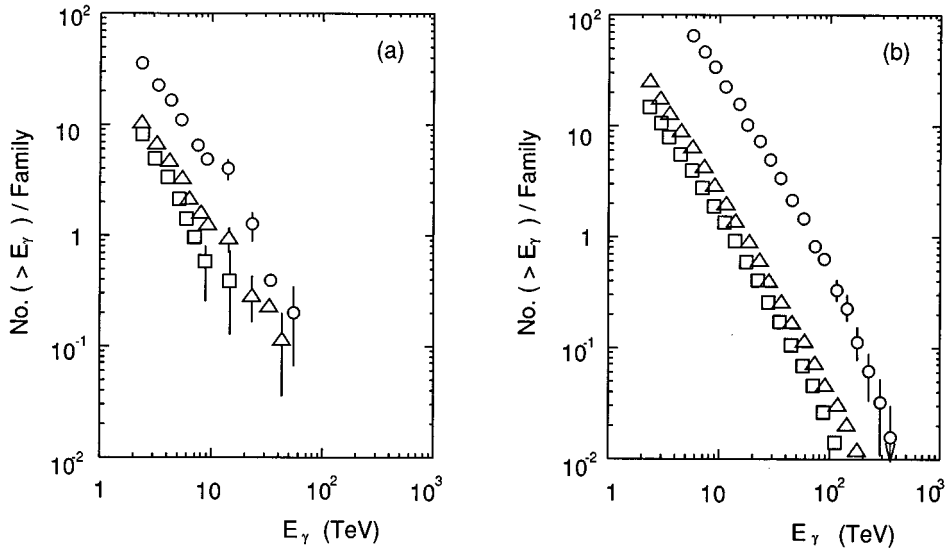

FIG. 6. Energy spectrum of γ rays in the family for three regions of the size of the accompanying air showers; $N_e=10^5$–10^6 (□), $N_e=10^6$–10^7 (△), and $N_e=10^7$–10^8 (○). (a) experimental data and (b) simulation.

on N_e in the experiment and in the simulation. In the simulation the center of the family is distributed randomly over one block of the emulsion chamber in order to take into account missing showers which fall outside the emulsion chamber, though the effect is found small.

It is seen in Fig. 11(a) that $\langle \Sigma E_\gamma \rangle$ of the experiment has a smaller value than that of the simulation. A similar tendency is seen by the experiment HADRON at Tien Shan [15], which is shown in Fig. 11(b). The discrepancy between the experiment and the simulation is found again in the relation between the family and the accompanied air shower.

The observed discrepancy, in Fig. 6 and in Fig. 11, indicates a more rapid energy dissipating process in the atmospheric propagation of cosmic rays at high energies. And the hypotheses for such a process under discussion are an increase of heavy components in the primary cosmic rays and the change of the nuclear interactions. The simulation shows, however, that the increase of iron component reduces the observed discrepancy only in part, because the simulated events of iron primaries have larger $\langle \Sigma E_\gamma \rangle$ than the value of the experiment, in the high-energy region $N_e>10^7$ [20]. Hence the change of nuclear interaction is necessary for the required rapid energy dissipating process, whether one assumes the increase of heavy primaries or not.

It may be worthwhile to note the following points regarding the above analysis.

(1) The analysis is free from the absolute intensity of the primary cosmic-ray spectrum.

(2) It is not the reason for the ineffectiveness of the iron component to $\langle \Sigma E_\gamma \rangle$ that most of the families, produced by the iron component, disappear in the atmosphere before arriving at the chamber, because the primary cosmic rays produce always the visible families in the region $N_e>10^7$, as was discussed in Sec. II.

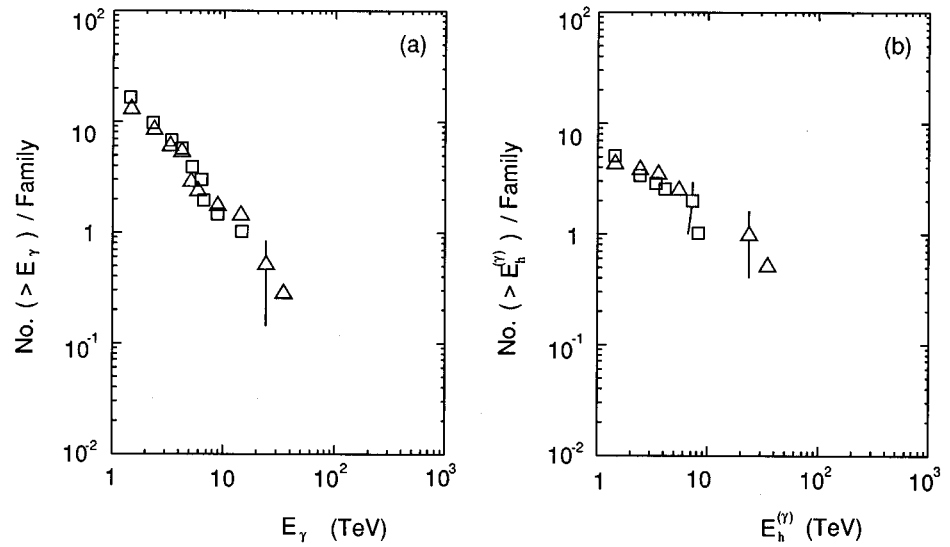

FIG. 7. Energy spectrum of γ rays (a) and hadrons (b) in the family for two groups of families. $E_h^{(\gamma)}$ in (b) is the visible energy of the hadron-induced shower. □, families with ΣE_γ=46.4–100 TeV and $N_e=10^5$–10^6; △, families with ΣE_γ=46.4–100 TeV and $N_e=10^6$–10^7.

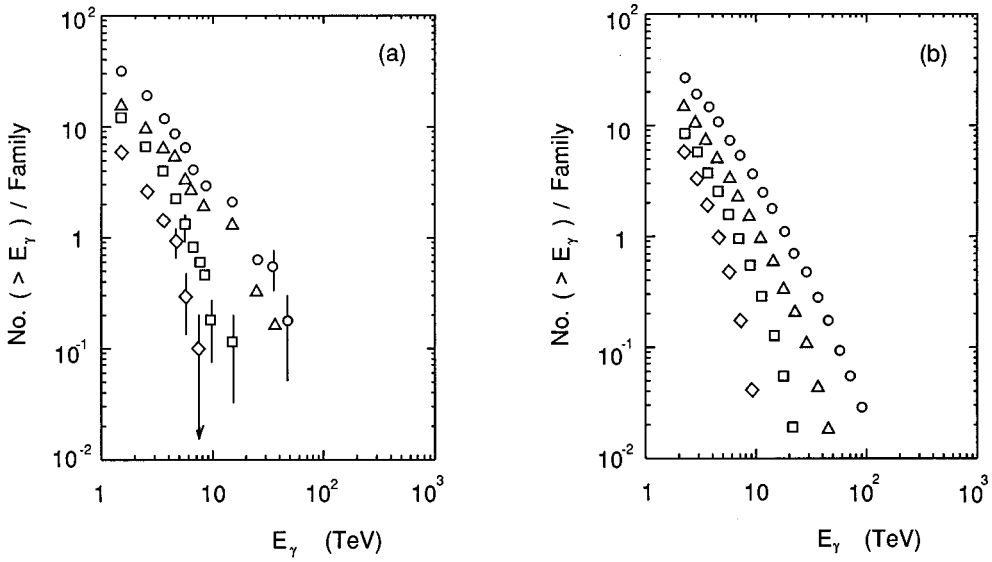

FIG. 8. Energy spectrum of γ rays in the family for four regions of ΣE_γ, without clssifying the data by N_e of the accompanying air shower. (a) and (b) are by the experimental data and by the simulation. ◇, $10 \leqslant \Sigma E_\gamma$ (TeV)<21.5; □, $21.5 \leqslant \Sigma E_\gamma$ (TeV)<46.4; △, $46.4 \leqslant \Sigma E_\gamma$ (TeV)<100; ○, $100 \leqslant \Sigma E_\gamma$ (TeV)<215.

(3) For the 47 families with accompanying air showers, the family centers always coincide with the core position of air showers within the experimental error. Hence there is no possibility that the families are produced locally at the periphery of the large air showers.

Figures 11(a) and (b) show that the experimental values of $\langle \Sigma E_\gamma \rangle$, at Mt. Chacaltaya and at Tien Shan, are similar in spite of the difference of altitudes, while the simulation shows that $\langle \Sigma E_\gamma \rangle$ at Mt. Chacaltaya is 2–3 times as large as that at Tien Shan. The reason for it may be attributed to the fact that the energies of γ rays are overestimated in the HADRON experiment, because the ΣE_γ spectrum at Tien Shan is not consistent with those at Mt. Chacaltaya and at Mt. Fuji.

D. Production spectrum of ΣE_γ

It is important to see what kind of families are produced by the air showers of a fixed size, or, more specifically, the distribution of ΣE_γ at a fixed value of N_e:

$$\varphi(x,N_e)dx \quad \text{with} \quad x=\Sigma E_\gamma .$$

It can be observed in Fig. 10 directly along a fixed value of N_e, if the statistics of the events is large enough and if the largest part of the distribution exists above the threshold of ΣE_γ. However unfortunately our experiment satisfies neither of the conditions. Hence, we will discuss it in another way.

The distribution can be expressed approximately by a single variable of $\Sigma E_\gamma / N_e^\delta$, because we have $\Sigma E_\gamma \propto E_0^\delta$ approximately. That is,

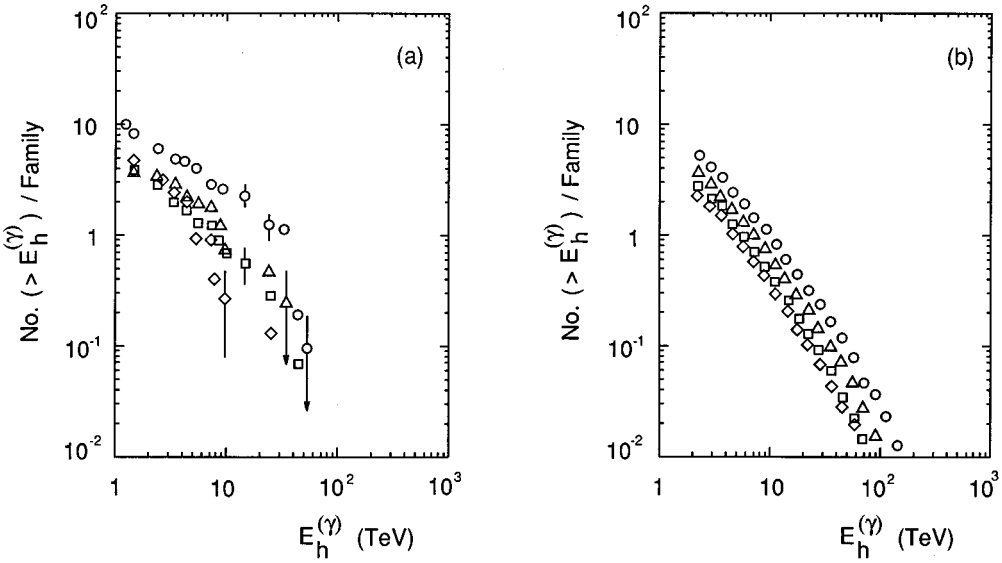

FIG. 9. Energy spectrum of hadrons in the family for four regions of ΣE_γ. The energy in the figure $E_h^{(\gamma)}$ is the visible energy of the hadron-induced shower. (a) and (b) are by the experimental data and by the simulation. ◇, $10 \leqslant \Sigma E_\gamma$ (TeV)<21.5; □, $21.5 \leqslant \Sigma E_\gamma$ (TeV)<46.4; △, $46.4 \leqslant \Sigma E_\gamma$ (TeV)<100; ○, $100 \leqslant \Sigma E_\gamma$ (TeV)<215.

$$\varphi(x,N_e)dx=\phi\left(\frac{x}{N_e^{\delta}}\right)\frac{dx}{N_e^{\delta}}.$$

The exponent δ assures the difference of the exponent between ΣE_γ spectrum and N_e spectrum. That is, the ΣE_γ spectrum is obtained as

$$\int \phi\left(\frac{x}{N_e^{\delta}}\right)\frac{dx}{N_e^{\delta}}\,\gamma I_0\left(\frac{N_e}{N_0}\right)^{-\gamma-1}\frac{dN_e}{N_0}=\beta I_0 x^{-\beta-1}dx\int y^{\beta}\phi(y)dy \quad \text{with } \beta=\frac{\gamma}{\delta} \text{ and } y=\frac{x}{N_e^{\delta}},$$

where $\gamma I_0(N_e/N_0)^{-\gamma-1}dN_e/N_0$ (with $\gamma=1.8$) is the N_e spectrum of the air showers. The integral spectrum of x $(=\Sigma E_\gamma)$ has the exponent β. We assume $\delta=1.44$, because $\beta=1.25$ by the experiment.

We will discuss the distribution of $\Sigma E_\gamma/N_e^{\delta}$, which corresponds to

$$\phi(y)dy \quad \text{with } y=\frac{\Sigma E_\gamma}{N_e^{\delta}}.$$

It means seeing the distribution of the events in Fig. 10 by rotating the y axis from the vertical line to the slant line of $\Sigma E_\gamma \propto N_e^{\delta}$.

The y distribution of the present experiment, shown in Fig. 12(b), have the maxima between $y=10^{-8}$ and $y=10^{-7}$. Naturally the value $\langle y\rangle=1.0\times10^{-8}$ TeV reproduces the relation between both spectra of ΣE_γ and N_e, Fig. 4 and Fig. 5, consistently. The distributions of the experiment [Fig. 12(b)] are broad compared with those of the simulation [Fig. 12(c)] where the events of proton primaries are sampled. It shows that the families are produced not only by protons (with the UA5 algorithm of nuclear interactions in the atmosphere) but also by other processes. For example, the families produced by iron primaries contribute to the left-hand side part of the distribution.

IV. SUMMARY AND DISCUSSION

(i) The observation of families and accompanied air showers is carried out at Mt. Chacaltaya (5200 m) by operating the emulsion chamber and the air shower array simultaneously. It is the role of the present experiment to mediate the air shower experiment and the emulsion chamber experiment, both of which have accumulated a lot of data independently.

The analysis is made for 47 families of $\Sigma E_\gamma \geqslant 10$ TeV with accompaniment of air showers, which are the data during the first 7 years (1979–1986) of the experiment. Principal conclusions of the present experiment are the following.

(1) Energy spectra of γ rays in one family are approximately the same, when the families are parametrized by ΣE_γ, irrespective of the size of the accompanied air shower. It is also the case for the hadrons in the family. It means that the family is produced deep in the atmosphere by a small number (one or two) of interactions of high-energy hadrons in the air shower.

(2) The feature of the families is reproduced well by the present simulation code, when the families are parametrized by ΣE_γ.

(3) There is a discrepancy between the experimental data and the simulation of current assumptions, which is seen in Fig. 6 and Fig. 11. For example, in the relation of $\langle\Sigma E_\gamma\rangle$ vs N_e in Fig. 11, $\langle\Sigma E_\gamma\rangle$ of the experiment is smaller appreciably than that of the simulation in the region $N_e>5\times10^6$. It indicates further energy dissipation in the atmospheric propagation of cosmic rays in the high-energy region $E_0>10^{16}$ eV, such as the heavy composition of the primary cosmic rays, the change of the nuclear interaction, etc. The simulation shows that the heavy composition reduces the observed discrepancy only in part. Therefore the change of nuclear interaction is necessary whether one assumes the increase of heavy primaries or not. This conclusion is free from the absolute intensity of the primary cosmic rays.

(ii) Taking into account the fact that the nuclear interaction model, assumed in the present simulation code, reproduces the violation of the Feynman scaling law consistently with the data by the accelerator experiments (at $\sim10^{14}$ eV), it is not easy to assume a much stronger violation of the law in the energy region $E_0>10^{16}$ eV. Hence it is more probable to assume that another channel, such as the production of Centauro species [27], opens in the nuclear interactions of high energies besides the channel of ordinary multiple particle production which is characterized by the pion dominance and small $\langle p_T\rangle$ value ($\sim$0.4 GeV/c) of produced particles.

(iii) If one applies Glauber theory [28] to hadron-air collisions in the simulation, one gets a larger value of the inelasticity ($\langle K\rangle=0.62$) and a longer collision mean free path than those assumed in the present simulation. The former

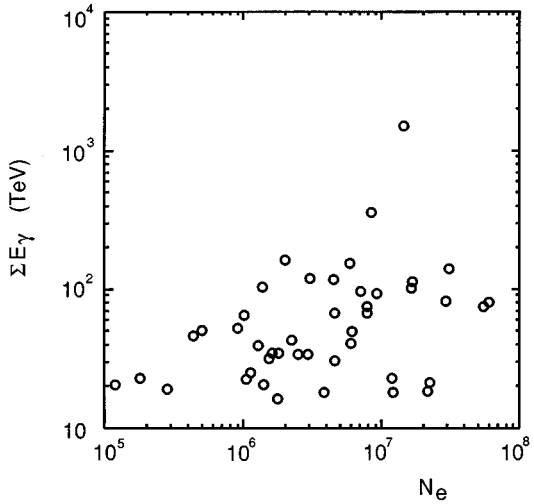

FIG. 10. Diagram between ΣE_γ (the total observed energy in the family) and N_e (the size of the air shower).

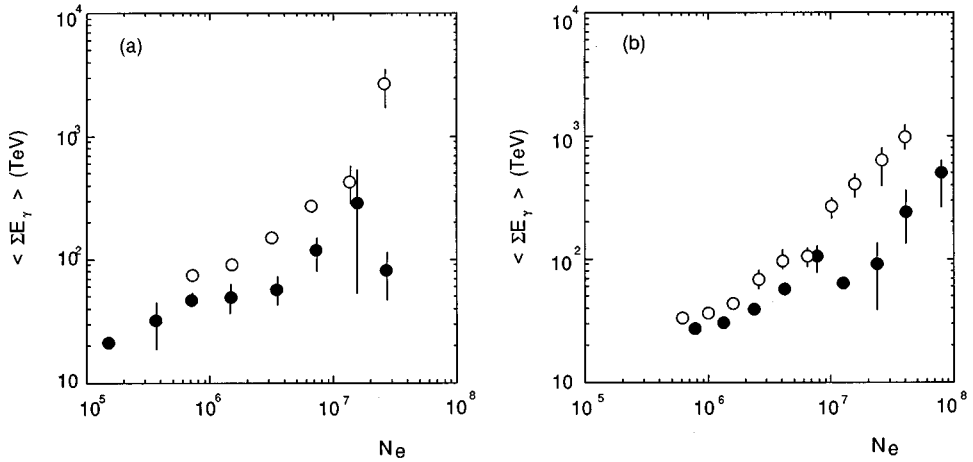

FIG. 11. Correlation between $\langle \Sigma E_\gamma \rangle$ (the average value of ΣE_γ) and N_e. (a) and (b) are by the present experiment and by the HADRON experiment. The full circles are by the experiment and the open circles by the simulation.

makes the energy dissipation larger, while the latter smaller. Hence the simulation code which takes the above alternative into account, gives similar values to the quantities discussed in the present paper. Details of the analysis by the code of the above alternative will be discussed elsewhere.

(iv) The relation between $\langle \Sigma E_\gamma \rangle$ and N_e is discussed by the ASγ experiment in Ref. [29]. It shows that $\langle \Sigma E_\gamma \rangle$ is almost constant and ~30 TeV over the size range of $N_e = 10^{4.5}$–$10^{7.5}$, which is nothing but the threshold effect of ΣE_γ. The high-energy region where air showers are accompanied by visible families without exception, has not been reached yet by ASγ experiment, due to the low altitude of the experimental site and/or the small area of the emulsion chamber. It is one of the reasons why the advantages of the simultaneous observation is taken little in their analysis, and why they had to devote much effort to couple families with air showers [5,7].

(v) We will not propose at present any model of the primary cosmic-ray composition but assume that it does not change so drastically from that of the lower energy region. It is because the estimation depends critically on the model of nuclear interaction, the detail of which is not clear yet and is to be elucidated urgently.

(vi) It is one of the advantages of the simultaneous observation of families and the accompanied air showers that one can select the events of low production height. Those events are characterized by the small values of $N_e/\Sigma E_\gamma$, (i.e., the events in the left-upper region in Fig. 10) and of the age parameter s of the air shower. For these events we can assume that the incident particles are nucleons which penetrate deep in the atmosphere, and that the families and the accompanied air showers are initiated by the same interactions. On such assumptions ΣE_γ of the family and N_e of the accompanied air shower enables us to estimate the production height and the primary energy of the event consistently.

Second, taking into account the fact that the family is produced mainly by one or two interactions of high-energy hadrons in the air shower, which is one of the conclusions of the present paper, the distribution of ΣE_γ's along the fixed value of N_e in Fig. 10 reflects the energy spectrum of hadrons produced in the nuclear interaction to initiate the air shower. It enables us to study nuclear interactions at the fixed energy in the energy region $E_0 > 10^{16}$ eV.

These items will be reported elsewhere with a better statistics of the events.

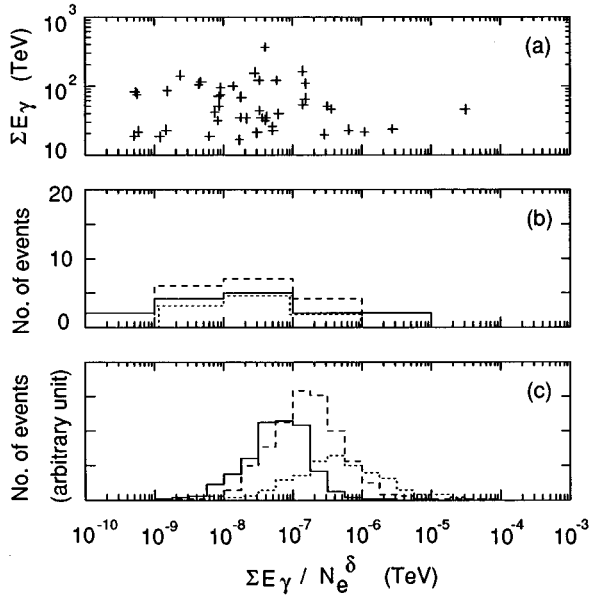

FIG. 12. The distribution of $y = \Sigma E_\gamma / N_e^\delta$. (a) Scatter plot of ΣE_γ of the families and $y = \Sigma E_\gamma / N_e^\delta$ where N_e is the size of the air shower. ΣE_γ is proportional to N_e^δ approximately. (See the text in Sec. IV.) (b) Histograms of $y = \Sigma E_\gamma / N_e^\delta$ for the events with a certain values of ΣE_γ, by the experiment. Solid line, $10 \leqslant \Sigma E_\gamma$ (TeV) < 31.6; dashed line, $31.6 \leqslant \Sigma E_\gamma$ (TeV) < 100; dotted line, $100 \leqslant \Sigma E_\gamma$ (TeV). (c) The same as (b) by the simulation of proton primaries. The total area under the histograms is normalized to the histogram in (b).

ACKNOWLEDGMENTS

The authors wish to express their gratitude to the financial support by the Japan Society for the Promotion of Science, which made it possible to realize this international collaboration. This experiment was also supported partly by the International Scientific Research Program and the Scientific Research Funds of the Ministry of Education, Science and Culture in Japan, by the Institute for Cosmic Ray Research,

University of Tokyo, and by the Nissan Science Foundation. The authors are indebted to the Bolivian staff of the Cosmic Ray Laboratory at Mt. Chacaltaya, in particular, R. Anda, O. Villegas, A. Velarde who were/is the director of Instituto de Investigaciones Fisicas, Universidad Mayor de San Andres, to which the Laboratory belongs. They are also grateful to Professor S. Okamoto, the former President of Saitama University, Professor T. Okumura of Saitama University, Professor Masaharu Machida, the former President of Yamanashi University, and Professor S. Miyake, the former director of the Institute for Cosmic Ray Research, for their continuous encouragement. They thank Professor Masaru Machida for his contribution at the early stage of this experiment. The data processing was made by FACOM M780 at the Computer Room, Institute for Nuclear Study, University of Tokyo, by ACOS-6 at the Information Processing Center of Yamanashi University, and by HITAC at the Information Processing Center of Saitama University. The x-ray films and nuclear emulsions were developed at facilities of Institute for Cosmic Ray Research, University of Tokyo.

APPENDIX: UA5 SIMULATION ALGORITHM

The UA5 algorithm is the simulation logic, developed by the UA5 Collaboration [24], to reproduce the data of multiple-particle production, which are observed by their detectors of streamer chamber at CERN SPS $\bar{p}p$ collider at $\sqrt{s}=53$, 200, 546, and 900 GeV. It consists of the codes of GENCL and DIFF. The former is for a nonsingle-diffractive process, and assumes basically the production and subsequent isotropic decay of small hadron clusters. The latter is for a single-diffractive process, the cross section of which is assumed to be 19% of the total inelastic cross section.

We will give below some comments on the characteristics of the UA5 algorithm, relevant to cosmic-ray experiments.

1. Inelasticity

In the UA5 algorithm the inelasticity is not the input but the output of the algorithm. The inelasticity distribution in the laboratory system is approximately uniform between 0.1 and 0.9, because the x distribution of the leading particle in the center-of-mass system is approximately uniform between 0.1 and 0.9. One should keep it in mind that the UA5 algorithm predicts the inelasticity of $\langle K\rangle=0.4$ in the laboratory system at $E_0=1.5\times10^{14}$ eV (or $\sqrt{s}=546$ GeV), indicating a decreasing inelasticity with the incident energy.

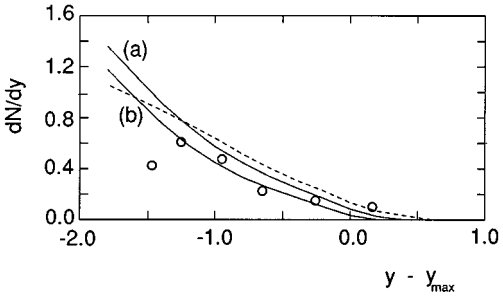

FIG. 13. Rapidity density of charged particles in the forward region. The dotted line is the scaling distribution, and the full lines, (a) and (b), are the prediction by the UA5 simulation algorithm at $\sqrt{s}=200$ and 900 GeV, respectively. The open circles are the data by the UA7 Collaboration (at $\sqrt{s}=630$ GeV), where $\sigma_{\rm inel}=49.0$ (mb) and $n_{\rm charged}/n_{\pi^0}=2.0$ are assumed.

2. Violation of the Feynman scaling law in the forward region

Our discussion is made in terms of the rapidity distribution $dN/dy\equiv(1/\sigma_{\rm inel})d\sigma/dy$, because it is equivalent to the discussion in terms of the x distribution owing to the relation $dN/dy=xdN/dx$. Figure 13 shows the rapidity distributions of produced particles in the forward region at different energies, predicted by the UA5 algorithm. The distributions show clearly the violation of the Feynman scaling law in the forward region, and are consistent with the data of the UA7 Collaboration [30]. To convert the rapidity distribution of π^0's, observed by the UA7 Collaboration, into that of the charged particles, $n_{\rm charged}/n_{\pi^0}=2.0$ and $\sigma_{\rm inel}=49.0$ mb are assumed.

One should notice that the statement that a certain interaction model reproduces the data by the UA5 Collaboration does not mean *a priori* that it reproduces the experimental data in the forward region, for example those by the UA7 Collaboration, because the UA5 data concern only the central region.

[1] Pamir Collaboration, Mt. Fuji Collaboration, and Chacaltaya Collaboration, S. G. Bayburina *et al.*, Nucl. Phys. **B191**, 1 (1981); Chacaltaya and Pamir Collaborations, L. T. Baradzei *et al.*, *ibid*. **B370**, 365 (1992).

[2] K. Greisen, Annu. Rev. of Nucl. Sci. **10**, 63 (1960).

[3] Yu. A. Smorodin, M. V. Solovyev, R. A. Antonov, L. T. Baradzei, V. V. Rykov, E. A. Kanevskaya, A. V. Apanasenko, S. I. Tulinova, and O. W. Sorokin, in *Proceedings of the 9th International Cosmic Ray Conference*, London, England, 1965, edited by A. C. Stickland (The Institute of Physics and Physical Society, London, 1965), Vol. 2, p. 827.

[4] T. Matano, M. Machida, and K. Ohta, Acta Phys. Hung. **29**, 451 (1970); T. Matano, M. Machida, K. Ohta, I. Imai, M. Nagayasu, I. Tsushima, N. Kawasumi, K. Honda, K. Hashimoto, C. Aguirre, R. Anda, R. Debbe, and C. Navia, in *Proceedings of the 17th International Cosmic Ray Conference*, Paris, France, 1981 (CEN, Saclay, 1981), Vol. 11, pp. 314 and 318; T. Matano, M. Machida, I. Imai, M. Nagayasu, K. Nagasaki, I. Tsushima, N. Kawasumi, K. Honda, K. Hashimoto, N. Martinic, R. Anda, R. Debbe, J. Zapata, L. Siles, P. Miranda, and C. Aguirre, in *18th International Cosmic Ray Conference*, Proceedings, Bangalore, India, 1983, edited by N. Durguprasad *et al.* (TIFR, Bombay, 1983), Vol. 11, p. 338; T. Matano, M. Machida, I. Tsushima, N. Kawasumi, K. Honda, K. Hashimoto, C. Navia, N. Martinic, and C. Aguirre, in *Proceedings of the 19th International Cosmic Ray Conference* La Jolla, California, 1985, 296 edited by F. C. Jones *et al.*, NASA Conf. Publ. 2376 (Goddard Space Flight Center, Greenbelt,

MD, 1985), Vol. 6, p. 296; T. Matano, T. Kobata, K. Mori, N. Inoue, I. Tsushima, N. Kawasumi, K. Honda, K. Hashimoto, N. Martinic, A. Reguerin, R. Ticona, and C. Aguirre, in *Proceedings of the 21st International Cosmic Ray Conference*, Adelaide, Australia, 1989, edited by R. J. Protheroe (Graphic Services, Northfield, South Australia, 1990), Vol. 8, p. 174; N. Kawasumi, K. Honda, I. Tsushima, K. Hashimoto, K. Mori, N. Inoue, R. Ticona, T. Matano, N. Martinic, Z. Aliaga, A. Reguerin, and C. Aguirre, in *Proceedings of the 22nd International Cosmic Ray Conference*, Dublin, Ireland, 1991, edited by M. Cawley *et al.* (Dublin Institute For Advanced Studies, Dublin, 1992), Vol. 4, p. 253; N. Kawasumi, I. Tsushima, K. Honda, K. Hashimoto, T. Matano, K. Mori, N. Inoue, R. Ticona, N. Martinic, Z. Aliaga, A. Reguerin, and C. Aguirre, in *Proceedings of the International Workshop on Super High Energy Hadron Interactions*, Tokyo, Japan, 1991, edited by Y. Fujimoto *et al.* (Waseda University, Tokyo, 1991), p. 306; N. Kawasumi, I. Tsushima, K. Honda, K. Hashimoto, T. Matano, K. Mori, N. Inoue, R. Ticona, A. Ohsawa, M. Tamada, N. Martinic, Z. Aliaga, A. Reguerin and C. Aguirre, in *Very High Energy Cosmic Ray Interactions*, Proceedings of the International Symposium, Ann Arbor, Michigan, 1992, edited by L. W. Jones, AIP Conf. Proc. No. 276 (AIP, New York, 1993), p. 88; N. Kawasumi, I. Tsushima, K. Honda, K. Hashimoto, T. Matano, K. Mori, N. Inoue, R. Ticona, A. Ohsawa, M. Tamada, N. Ohmori, N. Martinic, N. Gironda, F. Osco, and C. Aguirre, in *Proceedings of the 23rd International Cosmic Ray Conference*, Calgary, Canada, 1993, edited by R. B. Hicks *et al.* (World Scientific, Singapore, 1994), Vol. 4, p. 104; N. Kawasumi, I. Tsushima, K. Honda, K. Hashimoto, T. Matano, K. Mori, N. Inoue, A. Ohsawa, M. Tamada, N. Ohmori, N. Martinic, R. Ticona, N. Gironda, F. Osco, and C. Aguirre, in *Proceedings of the VIII International Symposium on Very High Energy Cosmic Ray Interactions*, Tokyo, Japan, 1994, edited by Y. Fujimoto *et al.* (Waseda University, Tokyo, 1994), p. 283.

[5] S. Dake, Y. Hatano, M. Hazama, K. Jitsuno, K. Nishikawa, M. Sakata, and Y. Yamamoto, Acta Phys. Hung. **29**, 671 (1970); S. Dake, M. Hazama, K. Jitsuno, K. Nishikawa, M. Sakata, Y. Yamamoto, and Y. Hatano, Nuovo Cimento B **41**, 55 (1977); M. Sakata, Y. Yamamoto, and S. Dake, *ibid*. A **70**, 297 (1982); Y. Fukushima, C. Hamayasu, T. Mitsumune, To. Saito, M. Sakata, M. Shima, Y. Yamamoto, S. Dake, M. Kawamoto, M. Kusunose, N. Ohmori, K. Kasahara, T. Shirai, S. Torii, and N. Hotta, Phys. Rev. D **39**, 1267 (1989).

[6] D. S. Adamov, V. V. Arabkin, K. V. Barkalov, N. G. Vildanov, A. G. Duvoby, A. D. Erlykin, B. B. Kadirsisov, S. K. Machavariani, A. A. Nam, N. M. Nesterova, S. I. Nikolsky, V. P. Pavljuchemko, P. V. Stavrev, K. V. Cherdyntseva, A. P. Chubenko, and S. B. Shaulov, in *Proceedings of the 20th International Cosmic Ray Conference*, Moscow, USSR, 1987, edited by V. A. Kozyarivsky *et al.* (Nauka, Moscow, 1987), Vol. 6, p. 144.

[7] M. Shima, To. Saito, M. Sakata, Y. Yamamoto, K. Kasahara, T. Yuda, S. Torii, and N. Hotta, Phys. Rev. D **39**, 1275 (1989).

[8] M. Shibata, Phys. Rev. D **24**, 1847 (1981).

[9] J. R. Ren *et al.*, Phys. Rev. D **38**, 1404 (1988).

[10] To. Saito, T. Yuda, K. Kasahara, S. Torii, N. Hotta, M. Sakata, and Y. Yamamoto, Astr. Part. Phys. **1**, 257 (1993).

[11] J. Kempa and J. Wdocwczyk, J. Phys. G **9**, 1271 (1983); in *Proceedings of the VIII International Symposium on Very High Energy Cosmic Ray Interactions* [4], p. 603.

[12] *Proceedings of the Meeting "Hadron Interactions in 10^{15}–10^{17} eV,"* Tokyo, Japan, 1993, edited by S. Hasegawa *et al.* (Waseda University, Tokyo, 1993), pp. 31 and 61.

[13] R. Feynman, Phys. Rev. Lett. **23**, 1415 (1969).

[14] T. Yuda, in *Proceedings of the 22nd International Cosmic Ray Conference* [4], Vol. 5, p. 313.

[15] V. V. Arabkin, S. I. Nikolsky, K. V. Cherdyntseva, and S. B. Shaulov, Lebedev Physical Institute Report No. FIAN 140, 1991 (unpublished); *Proceedings of the 22nd International Cosmic Ray Conference* [4], Vol. 4, pp. 269 and 273; S. B. Shaulov, in *Proceedings of the International Workshop on Super High Energy Hadron Interactions* [4], p. 228.

[16] Brazil-Japan Emulsion Chamber Collaboration, C. M. G. Lattes *et al.*, Prog. Theor. Phys. Suppl. **47**, 1 (1971).

[17] K. Greisen, *Progress in Cosmic Ray Physics* (North-Holland, Amsterdam, 1958), Vol. 3, p. 3; K. Kamata and J. Nishimura, Prog. Theor. Phys. Suppl. **6**, 93 (1958).

[18] F. Kakimoto, T. Kaneko, Y. Mizumoto, K. Suga, N. Inoue, K. Nishi, Y. Yamada, N. Tajima, E. Gotoh, H. Nakatani, H. Yoshii, R. Anda, C. Aguirre, P. K. MacKeown, K. Murakami, T. Hara, Y. Toyoda, and T. Maeda, J. Phys. G **9**, 339 (1983).

[19] J. Nishimura, *Handbuch der Physik* (Springer, Berlin, 1967), Vol. 46/2, p. 1.

[20] M. Tamada, J. Phys. G **20**, 487 (1994); in *Proceedings of the International Workshop on Super High Energy Hadron Interactions* [4], p. 263; in *VII International Symposium on Very High Energy Cosmic Ray Interactions* [4], p. 126.

[21] S. I. Nikolsky, *Proceedings of the 3rd Symposium on Cosmic Rays and Particle Physics*, Tokyo, 1984 (Institute for Cosmic Ray Research, University of Tokyo, 1984), p. 507.

[22] A. H. Hillas, in *Proceedings of the 16th International Cosmic Ray Conference*, Kyoto, Japan, 1979 (Institute for Cosmic Ray Research, Tokyo, 1979), Vol. 6, p. 13.

[23] E710 Collaboration, N. N. Amos, Phys. Lett. B **243**, 158 (1990).

[24] UA5 Collaboration, G. L. Alner *et al.*, Nucl. Phys. **B291**, 445 (1987).

[25] Y. Niihori, T. Shibata, I. M. Martin, E. H. Shibuya, and A. Turtelli, Jr., Phys. Rev. D **36**, 783 (1987).

[26] L. D. Landau and I. Pomeranchuk, Dokl. Akad. Nauk USSR **92**, 535 (1953); **92**, 735 (1953); A. B. Migdal, Phys. Rev. **103**, 1811 (1956).

[27] C. M. G. Lattes, Y. Fujimoto, and S. Hasegawa, Phys. Rep. **65**, 151 (1980); S. Hasegawa, *Proton-Antiproton Collider Physics*, edited by V. Barger, D. Cline, and F. Halzan, AIP Conf. Proc. No. 85 (AIP, New York, 1981), p. 500; Institute for Cosmic Ray Research Report No. 151-87-5, 1987 (unpublished).

[28] R. J. Glauber, Nucl. Phys. B**21**, 135 (1970).

[29] To. Saito, T. Yuda, K. Kasahara, S. Tori, N. Hotta, M. Sakata, and Y. Yamamoto, *Proceedings of the 22nd International Cosmic Ray Conference* [4], Vol. 4, p. 82.

[30] E. Pare, T. Doke, M. Haguenauer, V. Innocente, K. Kasahara, T. Kashiwagi, J. Kikuchi, S. Lanzano, K. Masuda, H. Murakami, Y. Muraki, T. Nakada, A. Nakamoto, and T. Yuda, Phys. Lett. B **242**, 531 (1990).